# Featured Surface Matching Method for Liver Image Registration

**SHU-TE SU [1], MING-CHIH HO [2], JIA-YUSH YEN [3], AND YUNG-YAW CHEN [1]**
[1]Department of Electrical Engineering, National Taiwan University, Taipei 10617, Taiwan
[2]Department of Surgery, National Taiwan University, Taipei 10617, Taiwan
[3]Department of Mechanical Engineering, National Taiwan University, Taipei 10617, Taiwan

Corresponding author: Yung-Yaw Chen (yychen@ntu.edu.tw)

**ABSTRACT** This research devises a method to match marker-less surfaces for liver image registration. Surgeons usually glean preoperative liver information, such as anatomy and the locations of liver tumors or large intrahepatic vessels, from preoperative liver images that are obtained using Computed Tomography (CT) scans, Magnetic Resonance Imaging (MRI) or ultrasound. During minimally invasive surgery, surgeons use a laparoscope to obtain information about the intraoperative liver surface and identify an intraoperative liver tumor or the locations of vessels using the preoperative information. However, the liver can be lifted, shifted, flipped, squeezed or turned over during surgery. These manual operations can lead to severe deformation, so it is difficult to identify the location of intraoperative liver tumors or vessels. It is also difficult to accurately remove a liver tumor while avoiding injury to large intrahepatic vessels. This research proposes a method to determine the location of intraoperative vessels or tumors. The proposed method uses CT scans to construct a preoperative biomechanical volume model and uses a novel surface matching method to determine the relationship between the preoperative and intraoperative surfaces. The preoperative volume model is deformed by the finite element model in terms of the relationship that is defined by the proposed surface matching method, so that it aligns with the intraoperative surface model and shows the location of intraoperative vessels and tumors. The method of target registration error is measured for an ex vivo porcine liver to validate the proposed method. The results show that the error in the internal marker (which represents the location of the tumor and the vessel) is $4.54 \pm 3.55$ mm and the error in the surface marker is $2.98 \pm 1.09$ mm, which demonstrates the feasibility and high degree of accuracy of the proposed method.

**INDEX TERMS** Finite element model, liver deformation, minimally invasive surgery, deformable image registration, surface matching.

## I. INTRODUCTION

Laparoscopic surgery brings many advantages such as less patient trauma, shorter recovery time and lower the risk of complication while comparing to open surgery. However, the surgeon must manually control the camera and tools within a narrow field of view. It is difficult to identify the intraoperative information such as vessels and tumors. Image registration is applied to resolve the problem. A preoperative organ image (surface plus internal information of the organ) is registered to an intraoperative organ image (partial surface or low resolution of 3D information) to produce the intraoperative information. Intraoperative information allows

the surgeon to identify critical locations during surgery. The technique is called image registration. Image registration researches try to resolve the problem in many perspective, such as image capture, image modeling, surface matching and image deformation algorithms, in either simulations or experiments. Surveys [1]–[4] show that current challenges are (1) real-time operation, (2) accuracy and (3) clinical trials. In terms of real-time computation, [5] shows that real-time computation is feasible using a parallel GPU architecture. Server processors, such as the Intel Xeon and the AMD EPYC, allow increased computing performance, so does NVIDIA GPU. Server processors and GPU will eventually allow real-time computation for image registration techniques. Accuracy has been improved using simulations or experiments that use a phantom, ex vivo organ or via clinical trials of improved

The associate editor coordinating the review of this manuscript and approving it for publication was Sudhakar Radhakrishnan [ID].

image registration methods, but the process is still not sufficiently accurate. The target accuracy for clinical trials is within 5 mm [1], which is a challenge for current image registration techniques.

For researches that register the preoperative image to the intraoperative image to predict the intraoperative locations of tumors or vessels, the image source that is used to construct the preoperative model and the intraoperative model must be selected. Commonly CT and MRI are used to capture preoperative images because these techniques offer high image resolution and low noise. They can also be captured from outside the operating room. The preoperative image is used to create an intervention plan and to construct the preoperative volume model. The volume model includes the surface and critical locations of tumors and vessels. During laparoscopic surgery, the intraoperative image is captured using an optical or non-optical method. A laparoscopic stereo camera, one of optical ways, captures partial images of the organ surface and gives no information about the location of tumors or vessels and the intraoperative image must be reconstructed before image registration.

Non-optical methods include ultrasound, cone-beam computed tomography (CBCT) [6] or open MR scanners [7]. These are used in a hybrid operating room to capture the intraoperative image. The slices of images form a complete 3D image of the organ. however, these methods feature low resolution or high noise, so image registration must occur after the intraoperative model is constructed. Then the location of the tumor or vessel is clearly identified. Thus, existing optical and non-optical methods require image registration to produce clear intraoperative information.

The preoperative and intraoperative models use different imaging modalities or coordinate systems so pre-registration, which is also called initial registration, is necessary to ensure that both modalities align. This usually involves rigid transformation using a fast algorithm.

The Iterative Closest Point (ICP) method aligns two point clouds rigidly by iteratively establishing the relationship between points to reduce the target registration error. There are many extended ICP methods. A modified ICP method, called Deformation-Identifying Rigid Registration (DIRR) [8], automatically rigidly registers an image so there is no need to manually set the initial condition. Another modified ICP [9] recursively minimize the registration error until it is less than a fixed threshold value. Convergent ICP [10] involves an improved ICP algorithm that increases accuracy when there is partial surface registration. Shape feature descriptors [11] uses a shape-based initial registration method that calculates the similarity of feature descriptors and uses the similarity and spatial correspondence to align both surfaces. All of the initial registration methods rigidly align the preoperative and the intraoperative images to allow a faster image registration process.

There are two parts in image registration techniques: surface matching and image deformation. Surface matching determines the relationship between the intraoperative and
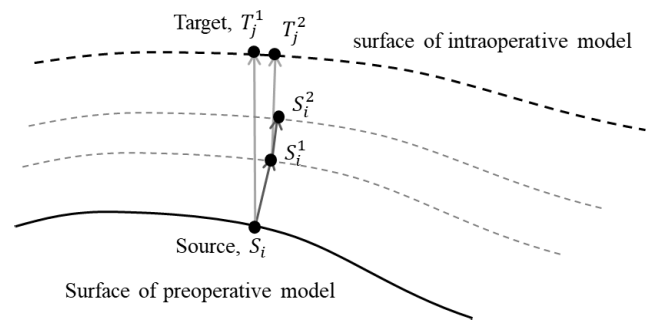


**FIGURE 1.** Closest point [8] determines the relationship between surfaces in the preoperative image and the intraoperative image using iterative, incremental normal vectors of minimal distance.

preoperative surfaces. Image deformation uses the relationship between surfaces that is identified during surface matching to deform the preoperative volume model. The internal tissue in the deformed volume model, such as tumors or vessels, is used to determine the location of intraoperative tumors or vessels.

There are many existing surface matching methods. The closest point [8] method is shown in FIGURE 1 and is a point-wise method that determines the relationship between surface points using normal-tangential space. It iteratively determines the surface displacement that is required to align both surfaces. The displacement of the preoperative surface points is the incremental normal vector of the minimum distance between the preoperative and intraoperative models. Hybrid similarity computation [12] determines the displacement using a weighted average of the similarity in the shape, the pose and the gas-pressure. Gaussian curvature [13] scores curvature on the organ surface and uses a set of cameras to determine the relationship between two surfaces.

The deformation model uses the result of surface matching to deform the preoperative volume model. Energy-error minimization [14] uses the biomechanical internal energy and the tracking energy. The registration is optimal if the internal forces equal the tracking forces. B-splines [15] and Thin-Plat Splines (TPS) [16] are common surface registration methods. Although neither method considers the biomechanical properties, they are still sufficiently accurate [17]. Finite Element (FE) [8], [14] regards the displacement of surface points as a boundary condition to deform the preoperative volume model. It calculates the internal energy and the external energy and achieves equilibrium to produce a deformed volume model. Another common method is the elastic method [18].

Section 2 of this research details the proposed method of image registration, especially the novel surface matching to determine the relationship between the preoperative surface and the intraoperative surface to reduce the image registration error. Section 3 shows and discusses the results for an experiment that use an ex vivo porcine liver. Section 4 concludes the proposed method.

## II. PROPOSED IMAGE REGISTRATION METHOD

This research proposes a novel surface matching method that aims at reducing image registration error. Accurate surface matching is essential because inaccurately aligned surfaces give a worse deformation result. The locational accuracy of internal tissue, such as vessel or tumor location, is important. The liver is one of organs that deforms dramatically during surgery. So this research uses the liver for image registration experiment. This research assumes that the intraoperative surface is reconstructed using optical methods or captured using non-optical methods. The reconstruction of the intraoperative partial surface is not discussed. The preoperative liver volume model (which includes the entire surface, vessels and tumor locations) and the intraoperative surface model (which includes a 3D image of the liver surface) are used for image registration. Image registration involves surface matching and image deformation. Surface matching determines the relationship between the preoperative surface and the intraoperative surface and image deformation uses this relationship to deform the preoperative volume model. The deformed model is a volume model and the location of vessels and tumors are inferred as intraoperative locations. The next time frame features the next 3D surface model and the previous deformed volume model becomes the new 3D volume model for image registration. The scope of this research is shown in FIGURE 2.
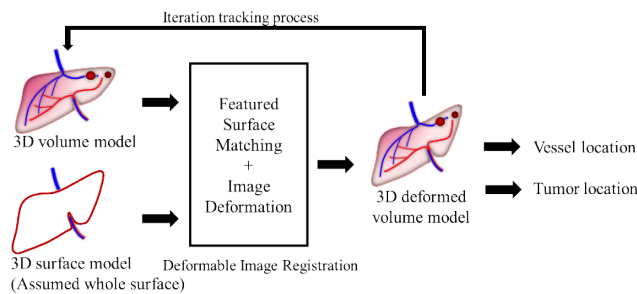


**FIGURE 2.** In this research, the 3D volume model is deformed to align with the 3D surface model by using featured surface matching method. The internal tissue in the 3D deformed volume model, such as tumors or vessels, is used to infer the location of intraoperative tumors or vessels.

The proposed method has two stages. The first stage involves image pre-registration, whereby the coordinate systems of the preoperative 3D volume model and the intraoperative 3D surface model are aligned using a rigid transformation. The second stage involves non-rigid image registration, whereby both surfaces are aligned using a Featured Surface Matching (FSM) method. This method uses curvature variation to create a leading point histogram as a local surface feature. A neighbor voting scheme is then based on local surface features to determine how the preoperative surface points be moved to align both surfaces. This displacement of points uses the Dirichlet boundary condition for finite element analysis to calculate the internal deformation of the preoperative 3D volume model. The location of vessels or

tumors in the deformed model then mimic the location of intraoperative vessels or tumors.

### A. PRE-REGISTRATION

The preoperative model and the intraoperative model use different coordinate systems so a weighted Iterative Closest Point (weighted-ICP) method is used to pre-register an image to ensure that both models use the same coordinate system. The cost function is calculated by rotating and translating the preoperative model with regard to the intraoperative model using weights. The optimal rigid transformation that aligns the preoperative model with the intraoperative model is obtained by minimizing the cost function:

$$E = \sum_{i=1}^{N} w_i \left| \left( R\vec{S}_i + T \right) - \vec{T}_j \right|^2 \qquad (1)$$

where $\vec{S}_i$ and $\vec{T}_j$ are the preoperative model and the intraoperative model, respectively and $R$ and $T$ are rotation and translation matrices, respectively. The initialized rotation matrix is an identity matrix and the translation matrix is a zero matrix. The weight $w_i$ is dependent on the distance between a point in the intraoperative model $\vec{T}_i$ and its centroid $\vec{C}$.

$$w_i = \begin{cases} 0, & if \ d\left(\vec{T}_i, \vec{C}\right) \geq k \cdot mean\left(d\left(\vec{T}_i, \vec{C}\right)\right) \\ \dfrac{1}{d\left(\vec{T}_i, \vec{C}\right)}, & else \end{cases}$$

$$(2)$$

where $k$ is manually-adjusted parameter for different scenarios and experiments. The weighted-ICP uses a K-D tree and is iterated around 1,000 times to ensure that the root mean square error is minimized.

### B. FEATURED SURFACE MATCHING METHOD

The FSM method measures the similarity of local surface features in the preoperative model and the intraoperative model and uses a neighbor voting scheme to determine the surface displacement. The surface displacement ensures that the preoperative model aligns with the surface of the intraoperative model.

The FSM method uses the curvature variation to build a local surface feature. 30% of points with a high curvature variation become the leading points. All of the curvature variations for the leading point and its neighbor points form a leading point histogram. The leading point histogram is a local surface feature. The preoperative leading point histograms and intraoperative leading point histograms are measured to determine high similarity points that feature leading point displacement. A neighbor voting scheme is used to determine the leading point displacement and to ensure that the displacement is in almost the same direction and distance as the neighbor leading points. The remainder of the points are trailing points. The trailing point displacement is the interpolation of the displacement of the neighbor leading points. Following subsections introduces FSM method in detail.

### 1) CURVATURE VARIATION

The curvature variation is used to obtain local surface features at points on a liver surface. A surface S is described as an implicit function, so for $f : \mathbb{R}^3 \to \mathbb{R}$

$$S = \left\{ x \in \mathbb{R}^3 \,|\, f(x) = 0 \right\} \tag{3}$$

A curvature tensor $\mathbb{C}(x, s)$ for a surface $S$ at each point $x \in S$ is calculated as (4).

$$f : \mathbb{C}(x, s) = \frac{\partial^2 f(x)}{\partial s^2} \tag{4}$$

where $s$ is the direction of the tangent at $x$. A curvature tensor is fully described by a $3 \times 3$ matrix of second order derivatives at point $x_0$ as:

$$\frac{\partial^2 f(x_0)}{\partial s^2} = s^T H s \tag{5}$$

where $H$ is a covariance matrix, which is also known as a Hessian matrix, of a surface function $f$, and can be expressed by:

$$H = \begin{bmatrix} \dfrac{\partial^2 f}{\partial x^2} & \dfrac{\partial^2 f}{\partial x \partial y} & \dfrac{\partial^2 f}{\partial x \partial z} \\ \dfrac{\partial^2 f}{\partial y \partial x} & \dfrac{\partial^2 f}{\partial y^2} & \dfrac{\partial^2 f}{\partial y \partial z} \\ \dfrac{\partial^2 f}{\partial z \partial x} & \dfrac{\partial^2 f}{\partial z \partial y} & \dfrac{\partial^2 f}{\partial z^2} \end{bmatrix} \tag{6}$$

A curvature tensor is fully described by a $3 \times 3$ matrix of second order derivatives. $\alpha$ is the angle that $s$ makes with the local coordinate axis at a fixed point $x_0$ on the surface S, curvature tensor (as function of $\alpha$) is extreme when:

$$\frac{\partial \mathbb{C}(x, s)}{\partial \alpha} = \frac{\partial}{\partial \alpha} \frac{\partial^2 f}{\partial s^2} = 0 \tag{7}$$

The non-trivial solution is

$$det(H - \lambda I) = 0 \tag{8}$$

Solving this second order equation in $\lambda$ yields three eigenvalues for curvature tensors, $\lambda_1$, $\lambda_2$, $\lambda_3$ and the respective eigenvectors for the curvature tensor are $s_1$, $s_2$, $s_3$, where $\lambda_1 > \lambda_2 > \lambda_3$.

The principal directions and values for the $3 \times 3$ curvature tensor can be calculated. The directions are those in which tensor has extreme values (max or min). These eigenvectors are orthogonal to each other. The values are the actual minimum and maximum values. That is,

$\lambda_1$, $s_1$ major eigenvalue and eigenvector

$\lambda_2$, $s_2$ medium eigenvalue and eigenvector

$\lambda_3$, $s_3$ minor eigenvalue and eigenvector

the curvature variation is defined as (9):

$$\kappa = \frac{\lambda_3}{\lambda_1 + \lambda_2 + \lambda_3} \tag{9}$$

where the interval of curvature variation is $\kappa \in \left[0, \frac{1}{3}\right]$ the curvature variation is $\frac{1}{3}$ if $\lambda_1 = \lambda_2 = \lambda_3$, the local surface is rugged, and not flat. If $\lambda_1 = \lambda_2 > \lambda_3$, $\lambda_1 > \lambda_2 = \lambda_3$ or $\lambda_1 > \lambda_2 > \lambda_3$, some directions may be flat. The greater the curvature variation, the more representative is the surface.

### 2) LEADING POINT DISPLACEMENT

Leading point is an outstanding point, and its curvature variation is top 30% of all surface points. The curvature variation of leading point and its neighbors can form a leading point histogram, which is used as a local surface feature. It is utilized to identify the surface point displacement from the preoperative model to the intraoperative model. The histogram plots the normalized number of neighbor points against curvature variation and is shown in FIGURE 3. The curvature variation is divided into several intervals with different bin sizes: [0.00, 0.02), [0.02, 0.05), [0.05, 0.10), [0.10, 0.16), [0.16, 1/3]. The curvature variation for the leading point and its neighbors that fall into each of the bins is normalized.
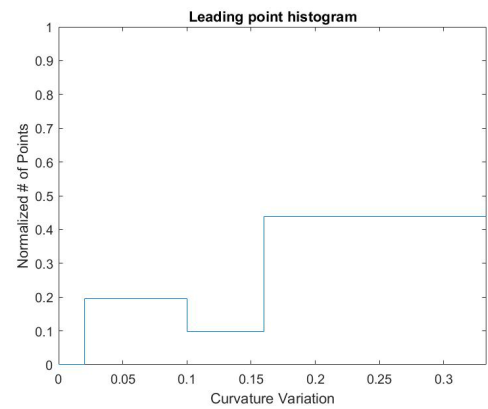
**FIGURE 3.** Leading point histogram to describe a local surface feature.

Curvature variation can change significantly on the liver surface, especially if a lobe is squeezed, flipped, or turned over. Using an iterative tracking process, the hypothesized local curvature variation does not change quickly between two iterations. The preoperative leading point histogram hist $(S)$ and the intraoperative leading point histogram hist $(T)$ have a high correlation coefficient $\rho$.

$$\rho = \frac{\sum_i \left[ hist\,(S_i) - \overline{hist\,(S)} \right] \left[ hist\,(T_i) - \overline{hist\,(T)} \right]}{\sqrt{\sum_i \left[ hist\,(S_i) - \overline{hist\,(S)} \right]^2 \sum_i \left[ hist\,(T_i) - \overline{hist\,(T)} \right]^2}} \tag{10}$$

where

$$\overline{hist\,(S)} = \frac{1}{N_S} \sum_i hist\,(S_i) \tag{11}$$

and

$$\overline{hist\,(T)} = \frac{1}{N_T} \sum_i hist\,(T_i) \tag{12}$$

where $N_S$ and $N_T$ are the total respective number of histogram bins in the preoperative model and the intraoperative model.

The similarity measurement determines leading point histograms in the preoperative and intraoperative models that are

similar using the correlation coefficient for the leading point histogram and the distance:

$$\varpi = \rho * \left(1 - \frac{d\,(S,\,T)}{d_{max}}\right) \qquad (13)$$

where $\varpi$ denotes the similarity between both leading point histograms, $\rho$ is the correlation coefficient for both leading point histograms, $d\,(S,\,T)$ is the distance between both leading points and $d_{max}$ is the maximum distance between the preoperative leading point and the intraoperative leading point. The ten most similar histograms are used as leading point displacement candidates and the remainder are ignored. The ten most similar histograms are normalized as:

$$\varpi_{normalized,k} = \frac{\varpi_k}{\sum_i \varpi_i} \qquad (14)$$

If local points on the liver surface have almost the same displacement between two iterations of the physical liver deformation, the neighbor voting scheme gives the displacement of the preoperative leading points using the normalized similarity and neighbor voting.

If the displacement of the leading point for a neighbor is almost the same as that for the preoperative leading points, the neighbor votes for the displacement using its normalized similarity, $\varpi_{ij}$. The displacement of the leading point is then the maximum value of the similarity measure for the displacement candidate, according to the sum of the neighbor's voting.

$$M^* = \arg\max_k \varpi_{normalized,k} * \left(\sum n_i \varpi_{ij}\right) \qquad (15)$$

where $M^*$ is the displacement of leading point using a neighbor voting scheme. If $n_i$ is 1, the neighbor votes for the displacement and if $n_i$ is 0, the neighbor does not vote.

### 3) FEATURED SURFACE MATCHING

The other points that are not leading points are called trailing points. The trailing points are in a flat region where it is difficult to infer the displacement based on local surface features. Trailing points assumed have the same displacement as leading points so the displacement of the trailing point, $\vec{T}$, is defined as the interpolation of displacement of the leading point displacement $\vec{L}_i$.

$$\vec{T} = \frac{1}{\sum_{i\in neighbor}\frac{1}{dist_i}} \sum_{i\in neighbor} \frac{1}{dist_i}\vec{L}_i \qquad (16)$$

where $dist_i$ is the distance between leading point and trailing point, for the leading point which is the neighbor of trailing point.

In order to ensure that both surfaces are matched, trailing point displacements are fine-tuned by morphological erosion or dilation of the minimal distance using the approaching factor is proposed in (17):

$$M = \alpha * D_{min} \qquad (17)$$

where M is the fine-tuned displacement of a trailing point, $\alpha$ is an approaching factor that is predefined as 0.1 and is adjusted
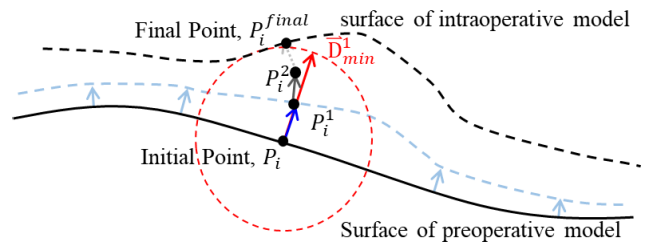


**FIGURE 4.** Trailing points are fine-tuned by iteratively morphological erosion or dilation of the minimal distance with an approaching factor.

for different scenarios and $D_{min}$ is the minimum distance on normal vector between the preoperative trailing points and the intraoperative points. Experience shows that this fine-tuning calculation requires around 5~30 iterations to yield the optimal surface matching result.

The proposed FSM method aligns the preoperative surface with the intraoperative surface by dividing surface points into leading points and trailing points. The leading point displacement is defined using a neighbor voting scheme with similarity measures and the trailing point displacement is the interpolation of the leading point displacements with a fine-tuning scheme. The leading point displacements and the trailing point displacements form a group of preoperative surface displacements that allow the preoperative surface to align with the intraoperative surface.

### C. CALCULATING THE LIVER DEFORMATION

This research uses the finite element model to calculate the liver deformation. The liver, tumors and vessels are formulated using a biomechanical model and the deformation calculation is solved using partial differential equations. The local control points and 3D volume deformation have biomechanical parameters. (18) is the strong form of the boundary condition problem:

$$\nabla \cdot \sigma = B \qquad (18)$$

where $\sigma$ represents the stress tensor and B denotes the external forces that act on the object. The liver is assumed to feature a linear relationship between stress ($\sigma$) and strain ($\varepsilon$), as (19):

$$\sigma = C\varepsilon \qquad (19)$$

where the stiffness matrix C and Young's modulus ($E$) and Poisson's ratio ($\upsilon$) are dependent. The strain tensor $\varepsilon$ is calculated as (20):

$$\varepsilon = \frac{1}{2}\left((\nabla u)^T + \nabla u\right) = Bu \qquad (20)$$

where u is the displacement field. Substituting (18) and (19) into (20) gives the displacement vector ($u$) as (21):

$$\frac{E}{2\,(1+\upsilon)}\nabla^2 u + \frac{E}{2\,(1+\upsilon)\,(1-2\upsilon)}\nabla\,(\nabla\cdot u) = B \qquad (21)$$

Galerkin weighted residuals and a linear basis function are used to solve (21). This system equation solves the Cartesian
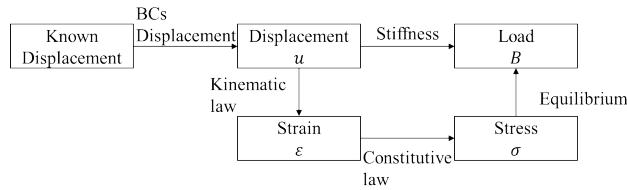
**FIGURE 5.** The finite element mechanism that is used for geometric transformation.

displacement u at every node in the tetrahedral mesh as:

$$[K]\{u\} = \{B\} \qquad (22)$$

where $\{u\}$ is the three-dimensional displacement for each node. To simulate soft-tissue deformation, the equation is solved by obtaining known displacement values for some nodes.

The FSM method calculates the optimal surface displacements that allow the preoperative model to align with the intraoperative model. The featured surface displacements are the inputs for the Dirichlet boundary condition for the finite element model computation. The output from the finite element model is the deformed volume model, for which the surface and the locations of tumors or vessels are the same as those for the intraoperative model.

## III. EXPERIMENT ON AN EX VIVO PORCINE LIVER

The proposed method is validated using an experiment on an ex vivo porcine liver. FIGURE 6(a) shows the preoperative ex vivo porcine liver. FIGURE 6(b) is the intraoperative ex vivo porcine liver, which is obtained by manual operations on the preoperative ex vivo porcine liver. There are three different combinations of manual operations: shifting, lifting and shifting and lifting. In the left lobe, the edge of liver is pulled 25 mm using a fishing-line to create a shift deformation. In the middle lobe, the liver is lifted 60 mm using a pad, which causes severe deformation. In the right lobe, the liver is first shifted 10 mm and then lifted 18 mm using a pad. Manual operations involving lifting and shifting are performed on the liver lobes to mimic surgical operations that use in minimally invasive surgery. Note that the left lobe is on the right-hand side of the figure and the right lobe is on the left side in FIGURE 6(a) and (b).

5 pinned markers, 10 surface markers and 26 internal markers are fixed on or inserted into the ex vivo porcine liver. 0.5mm nails are inserted close to the hepatic portal vein as pinned markers to mimic large blood vessels and are used to measure the accuracy of the pre-registration. 5mm plastic pearls are sewn on the surface of the ex vivo porcine liver as surface markers and are used to measure the accuracy of surface matching. 3mm metal balls are inserted into the ex vivo porcine liver as internal markers (by cutting, stuffing, and sewing) to mimic the locations of vessels and tumors and are used to measure the accuracy of the overall registration algorithm.
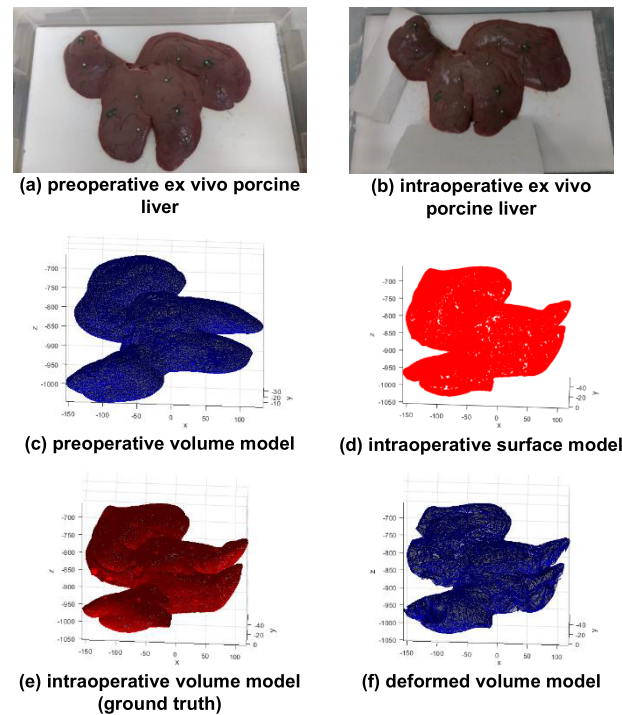


(a) preoperative ex vivo porcine liver



(b) intraoperative ex vivo porcine liver



(c) preoperative volume model



(d) intraoperative surface model



(e) intraoperative volume model (ground truth)



(f) deformed volume model

**FIGURE 6.** The experiment to validate the proposed method: (a) the preoperative ex vivo porcine liver includes 26 surface markers, 10 internal markers and 5 pinned markers, (b) the intraoperative ex vivo porcine liver is constructed using manual operations on the preoperative ex vivo porcine liver by lifting the right lobe 18 mm and shifting it 10 mm, lifting the middle lobes 60 mm and shifting the left lobe 25 mm, (c) the preoperative volume model is constructed using CT scans of the preoperative ex vivo porcine liver, (d) the intraoperative surface model is the surface part of the intraoperative volume model, (e) the intraoperative volume model is constructed using CT scans of the intraoperative ex vivo porcine liver and is a ground truth and (f) the deformed volume model is the output of the proposed method when the preoperative volume model is deformed with respect to the intraoperative surface model.

The preoperative volume model is shown in FIGURE 6(c) as a biomechanical model that is constructed from CT scans of the preoperative ex vivo porcine liver. A 3D marching cube algorithm [19] is used to create 3D mesh points for the entire contour of the preoperative ex vivo porcine liver, in order to create a surface mesh. A ten-node tetrahedral element (C3D10) is used to construct the internal mechanism for the liver, tumors and vessels. The mesh grid points are seeded in the liver, tumors and vessels to generate meshes. The element edges for the model are less than 1mm to increase accuracy and to decrease the possibility of distortion. The tissue properties for the liver, tumors and vessels are defined separately. An elastic finite element model often uses Young's modulus and Poisson's ratio to represent tissue properties. The parameters for Young's modulus and Poisson's ratio are given in [20], [21], Young's modulus and Poisson's ratio for the liver and tumor are 27KPa and 0.45, respectively. Young's modulus for a vessel is 0.62MPa and Poisson's ratio is 0.45. A biomechanical model is constructed using these parameters. Manually constructing the biomechanical model requires ~65 seconds (Intel Xeon CPU E5-1630 v3 @3.7GHz; DDR4 64.0 GB).

During minimally invasive surgery, only a part of the intraoperative surface is visible if a stereo camera is used. This research assumes that this partial surface is well reconstructed. This research skip the reconstruction problem. So the intraoperative surface model in FIGURE 6(d) shows the entire surface that is constructed using CT scans of the intraoperative ex vivo porcine liver.

The ground truth that is used to measure the accuracy of image registration must include both the liver surface and the locations of the three types of markers. The ground truth is obtained from biomechanical models of CT scans of the intraoperative ex vivo porcine liver. The parameters for the construction of the biomechanical model and the biomechanical parameters are the same as those that are used to model the preoperative ex vivo porcine liver.

Both the preoperative volume model and the intraoperative surface model are inputs for the proposed method. The output is the deformed volume model that is compared with the intraoperative ground truth using marker locations to measure the accuracy, as shown in FIGURE 6(f).

The results show that the computation time is ∼270 sec (Intel Xeon CPU E5-1630 v3 @3.7GHz; DDR4 64.0 GB), the pinned marker error is $1.05 \pm 0.85$ mm, the surface marker error is $2.98 \pm 1.09$ mm (initial error is $12.18 \pm 5.49$ mm) and the internal marker error is $4.54 \pm 3.55$ mm (initial error is $12.08 \pm 4.27$ mm).

The pinned marker error of $1.05 \pm 0.85$ mm shows that weighted-ICP is highly accurate for pre-registration. The surface marker error and the internal marker error feature two regions with large errors in the left lobe and in the middle lobe. The left lobe is shifted in two opposite directions. However, the liver was placed on Styrofoam and the friction between the liver and the Styrofoam inhibits the displacement of some portions. The FSM method regards flat bottom part as trailing points. The displacement of the trailing point (flat part) is the interpolation of the displacement of the neighboring leading points (curved part) so the FSM method does not account for friction. This produces large errors for the left lobes. In the middle lobe, the weight of heavy internal markers causes them to sink in different directions so error are large and the height of internal markers is lower than the computed result.

To determine registration errors in each lobe, FIGURE 9 shows the internal marker errors for all and each of the ex vivo porcine liver lobes. All registration errors are reduced from an initial error (IE) of $12.08 \pm 4.27$ mm to the target registration error (TRE) of $4.54 \pm 3.55$ mm, where IE is the error between the preoperative (after pre-registration) and the ground truth internal markers and TRE is the target registration error between the deformed internal markers and the ground truth internal markers. The left lobe (to verify shift operation) has an IE value of $10.39 \pm 3.26$ mm and this is reduced to a TRE of $4.73 \pm 3.22$ mm. The middle lobes (to verify lift operation) have an IE value of $14.09 \pm 4.66$ mm and this is reduced to a TRE of $4.51 \pm 4.11$ mm. The right lobe (to verify shift and lift operation) has an IE
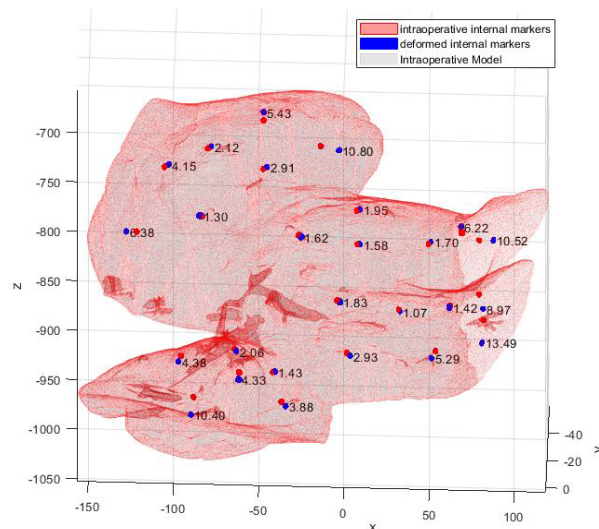


**FIGURE 7.** The distribution of the error for 26 internal markers: each error is annotated next to a marker.
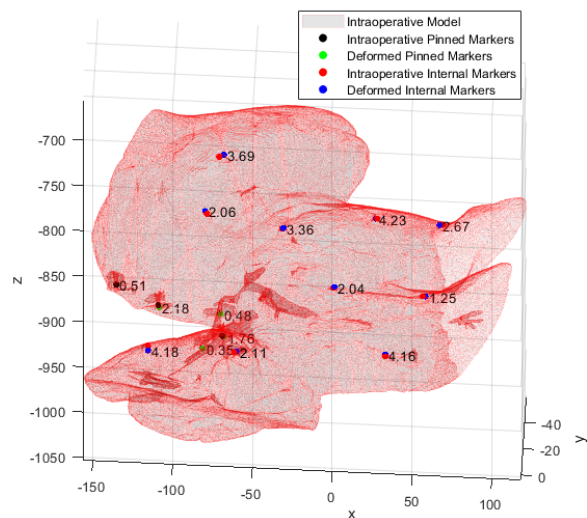


**FIGURE 8.** The distribution of the error for 5 pinned markers and 10 surface markers: each error is annotated next to a marker.

value of $9.70 \pm 2.25$ mm and this is reduced to a TRE of $4.41 \pm 3.18$ mm.

FIGURE 10 shows the IE value for each internal marker compare to the TRE. Almost all errors are reduced, except those for some markers that experience an opposite frictional force or the internal marker sinks in different directions. Markers that experience an opposite frictional force have an IE of $10.07 \pm 4.20$ mm, and this is reduced to a TRE of $8.25 \pm 2.74$ mm using the proposed method. For markers that sink in different directions, the errors are reduced from $18.34 \pm 5.31$ mm to $8.90 \pm 3.31$ mm using the proposed method. The proposed method can reduces both types of errors but it is not ideal. When both problems are skipped, the FSM method reduce an IE of $10.86 \pm 1.76$ mm to a TRE of $2.84 \pm 2.19$ mm and obtains high quality registration. This
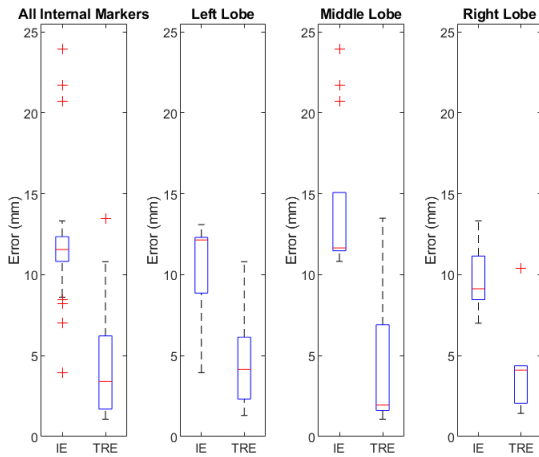
**FIGURE 9.** These box plots compare the IE and TRE for different areas: the left lobe with shift operations, the middle lobe with lift operations and the right lobe with both shift and lift operations.
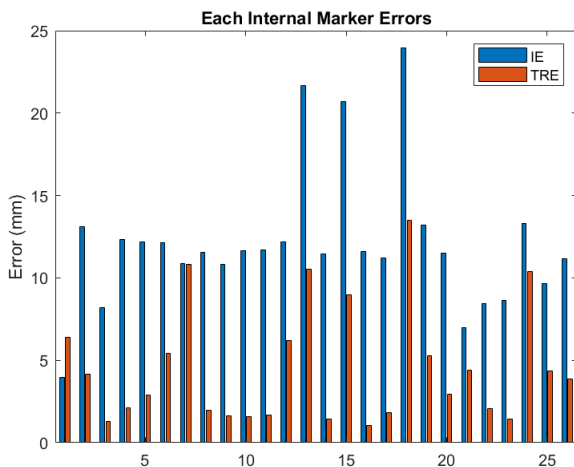


**FIGURE 10.** A comparison of the IE and TRE for the error for 26 internal markers: the error is reduced using the proposed method and image deformation.

**TABLE 1.** Units for magnetic properties.

|  | The Closest Point [8] | FSM |
|---|---|---|
| Surface TRE (mm) | 3.44 ± 1.66 | 2.98 ± 1.09 |
| Internal TRE (mm) | 5.73 ± 5.49 | 4.54 ± 3.55 |

shows friction and heavy marker sinks are challenges for the proposed method.

Table 1 compares the results for the FSM method and the closest point [8] method for the same dataset, pre-registration method and deformation calculation. The FSM performs better for the surface and internal TRE. The FSM method performs better for middle lobes that have severe deformations. An improved surface TRE means that fewer errors accumulate from the surface to the internal region, so the internal TRE is better.

## IV. CONCLUSION

This research proposes a marker-less featured surface matching (FSM) method, which determines the relationship between surface points on two surfaces of an organ. It is a point-wise, feature based method in Euclidean coordinate system. It uses a non-iterative image registration scheme that increases the accuracy of surface matching and decreases computation time.

The preoperative volume model is constructed using the preoperative organ image, it includes surface, tumors and vessels of the organ. The intraoperative surface model uses the intraoperative organ image, it usually a partial surface or low resolution of 3D information. This research assumes the intraoperative surface model is a reconstructed entire surface of the organ. The FSM method determines the relationship between surface points and the finite element model is used to establish the relationship between surface points as a Dirichlet boundary condition and to propagate the surface displacement into internal elements. This produces a deformed volume model that contains the locations of tumors and large blood vessels. The location information is helpful for the surgeon during minimally invasive surgery.

The proposed method is validated by an experiment that uses an ex vivo porcine liver. Using the proposed method for an ex vivo porcine liver experiment requires a computation time of ∼270 sec and there is a low surface marker error of 2.98 ± 1.09 mm while the initial error is 12.18 ± 5.49 mm. The internal marker error is 4.54 ± 3.55 mm while the initial error is 12.08 ± 4.27 mm. The validation result shows the feasibility of the proposed method, which is highly accurate and features a fast computation speed.

## REFERENCES

[1] S. Bernhardt, S. A. Nicolau, L. Soler, and C. Doignon, "The status of augmented reality in laparoscopic surgery as of 2016," *Med. Image Anal.*, vol. 37, pp. 66–90, Apr. 2017, doi: 10.1016/j.media.2017.01.007.

[2] S. Chakraborty, P. K. Patra, P. Maji, A. S. Ashour, and N. Dey, "Image registration techniques and frameworks: A review," in *Proc. Appl. Video Process. Surveill. Monitor. Syst., IGI Global*, 2017, pp. 102–114.

[3] S. Matl, R. Brosig, M. Baust, N. Navab, and S. Demirci, "Vascular image registration techniques: A living review," *Med. Image Anal.*, vol. 35, pp. 1–17, Jan. 2017.

[4] F. P. Oliveira and J. M. R. Tavares, "Medical image registration: A review," *Comput. Methods Biomech. Biomed. Eng.*, vol. 17, no. 2, pp. 73–93, 2014.

[5] Z. Ronaghi, E. B. Duffy, and D. M. Kwartowitz, "Toward real-time remote processing of laparoscopic video," *J. Med. Imag.*, vol. 2, no. 4, Dec. 2015, Art. no. 045002, doi: 10.1117/1.JMI.2.4.045002.

[6] P. Mountney, J. Fallert, S. Nicolau, L. Soler, and P. W. Mewes, "An augmented reality framework for soft tissue surgery," in *Medical Image Computing and Computer-Assisted Intervention—MICCAI*. Cham, Switzerland: Springer, 2014, pp. 423–431.

[7] N. Tsutsumi, M. Tomikawa, M. Uemura, T. Akahoshi, Y. Nagao, K. Konishi, S. Ieiri, J. Hong, Y. Maehara, and M. Hashizume, "Image-guided laparoscopic surgery in an open MRI operating theater," *Surgical Endoscopy*, vol. 27, no. 6, pp. 2178–2184, Jun. 2013, doi: 10.1007/s00464-012-2737-y.

[8] D. M. Cash, M. I. Miga, T. K. Sinha, R. L. Galloway, and W. C. Chapman, "Compensating for intraoperative soft-tissue deformations using incomplete surface data and finite elements," *IEEE Trans. Med. Imag.*, vol. 24, no. 11, pp. 1479–1491, Nov. 2005, doi: 10.1109/TMI.2005.855434.

[9] L.-M. Su, B. P. Vagvolgyi, R. Agarwal, C. E. Reiley, R. H. Taylor, and G. D. Hager, "Augmented reality during robot-assisted laparoscopic partial nephrectomy: Toward real-time 3D-CT to stereoscopic video registration," *Urology*, vol. 73, no. 4, pp. 896–900, Apr. 2009, doi: 10.1016/j.urology.2008.11.040.

[10] L. Maier-Hein, A. M. Franz, T. R. dos Santos, M. Schmidt, M. Fangerau, H. Meinzer, and J. M. Fitzpatrick, "Convergent iterative closest-point algorithm to accomodate anisotropic and inhomogenous localization error," *IEEE Trans. Pattern Anal. Mach. Intell.*, vol. 34, no. 8, pp. 1520–1532, Aug. 2012.

[11] T. R. dos Santos, A. Seitel, T. Kilgus, S. Suwelack, A.-L. Wekerle, H. Kenngott, S. Speidel, H.-P. Schlemmer, H.-P. Meinzer, T. Heimann, and L. Maier-Hein, "Pose-independent surface matching for intra-operative soft-tissue marker-less registration," *Med. Image Anal.*, vol. 18, no. 7, pp. 1101–1114, Oct. 2014, doi: 10.1016/j.media.2014.06.002.

[12] S. F. Johnsen, S. Thompson, M. J. Clarkson, M. Modat, Y. Song, J. Totz, K. Gurusamy, B. Davidson, Z. A. Taylor, D. J. Hawkes, and S. Ourselin, "Database-based estimation of liver deformation under pneumoperitoneum for surgical image-guidance and simulation," in *Medical Image Computing and Computer-Assisted Intervention—MICCAI*. Cham, Switzerland: Springer, 2015, pp. 450–458.

[13] M. R. Robu, P. Edwards, J. Ramalhinho, S. Thompson, B. Davidson, D. Hawkes, D. Stoyanov, and M. J. Clarkson, "Intelligent viewpoint selection for efficient CT to video registration in laparoscopic liver surgery," *Int. J. Comput. Assist. Radiol. Surg.*, vol. 12, no. 7, pp. 1079–1088, Jul. 2017, doi: 10.1007/s11548-017-1584-7.

[14] N. Haouchine, J. Dequidt, I. Peterlik, E. Kerrien, M.-O. Berger, and S. Cotin, "Image-guided simulation of heterogeneous tissue deformation for augmented reality during hepatic surgery," in *Proc. IEEE Int. Symp. Mixed Augmented Reality (ISMAR)*, Oct. 2013, pp. 199–208.

[15] T. Lange, S. Eulenstein, M. Hünerbein, and P.-M. Schlag, "Vessel-based non-rigid registration of MR/CT and 3D ultrasound for navigation in liver surgery," *Comput. Aided Surg.*, vol. 8, no. 5, pp. 228–240, Jan. 2003, doi: 10.3109/10929080309146058.

[16] F. L. Bookstein, "Principal warps: Thin-plate splines and the decomposition of deformations," *IEEE Trans. Pattern Anal. Mach. Intell.*, vol. 11, no. 6, pp. 567–585, Jun. 1989, doi: 10.1109/34.24792.

[17] A. Sen, B. M. Anderson, G. Cazoulat, M. M. McCulloch, D. Elganainy, B. A. McDonald, Y. He, A. S. R. Mohamed, B. A. Elgohari, M. Zaid, E. J. Koay, and K. K. Brock, "Accuracy of deformable image registration techniques for alignment of longitudinal cholangiocarcinoma CT images," *Med. Phys.*, early access, Jan. 20, 2020, doi: 10.1002/mp.14029.

[18] N. Haouchine, F. Roy, L. Untereiner, and S. Cotin, "Using contours as boundary conditions for elastic registration during minimally invasive hepatic surgery," in *Proc. IEEE/RSJ Int. Conf. Intell. Robots Syst. (IROS)*, Oct. 2016, pp. 495–500, doi: 10.1109/IROS.2016.7759099.

[19] W. E. Lorensen and H. E. Cline, "Marching cubes: A high resolution 3D surface construction algorithm," *ACM SIGGRAPH Comput. Graph.*, vol. 21, no. 4, pp. 163–169, Aug. 1987, doi: 10.1145/37402.37422.

[20] I. Peterlík, C. Duriez, and S. Cotin, "Modeling and real-time simulation of a vascularized liver tissue," in *Medical Image Computing and Computer-Assisted Intervention—MICCAI*, N. Ayache, H. Delingette, P. Golland, and K. Mori, Eds. Berlin, Germany: Springer, 2012, pp. 50–57.

[21] S. Umale, S. Chatelin, N. Bourdet, C. Deck, M. Diana, P. Dhumane, L. Soler, J. Marescaux, and R. Willinger, "Experimental *in vitro* mechanical characterization of porcine Glisson's capsule and hepatic veins," *J. Biomech.*, vol. 44, no. 9, pp. 1678–1683, Jun. 2011, doi: 10.1016/j.jbiomech.2011.03.029.
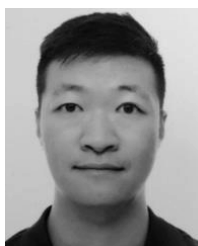
**SHU-TE SU** received the M.S. degree from the Department of Electrical Engineering, National Taiwan University, Taiwan, in 2009, where he is currently pursuing the Ph.D. degree. His current research interests include robot vision, pattern recognition, and deformable image registration.

**MING-CHIH HO** received the M.D. degree from the School of Medicine, National Taiwan University, and the Ph.D. degree in surgery from the College of Medicine, Institute of Clinical Medicine, National Taiwan University. He received his surgical training at the Department of Surgery, National Taiwan University Hospital, and completed visiting fellowships in liver transplantation at the University of Pittsburg Medical Center and the San Francisco Medical Center, University of California at San Francisco. He is currently a Professor with the Department of Surgery, College of Medicine, National Taiwan University, and the National Taiwan University Hospital, and the Director of the Surgical Department, National Taiwan University Hospital, Hsin-Chu Biomedical Park Branch. He specializes in the management liver cancer, liver transplantation, and abdominal diagnostic imaging. His current research interests focus primarily on liver cancer, liver transplantation, and hepatobiliary imaging.

**JIA-YUSH YEN** received the B.S. degree from National Tsing Hua University, Taiwan, in 1980, the M.S. degree from the University of Minnesota, USA, in 1983, and the Ph.D. degree from the University of California at Berkeley, Berkeley, in 1989, all in mechanical engineering.

He then joined the Mechanical Engineering Faculty, National Taiwan University, where he served as the Department Chair, the Director of the Tjing-Ling Industrial Research Institute, and the Dean of the College of Engineering, until 2017. He has also served as the Chair of the Automation Area for the Ministry of Science and Technologies, Taiwan, the President of the Chinese Institute of Automation Engineers (CIAE), Taiwan. He currently serves as the President of the Chinese Automatic Control Society, Taiwan, the Director of the NTU Research and Development Center for Medical Devices, and the NTU Research Center for Intelligent Machines. He had also served as a Consultant for many companies and institutes. His research interests are in the areas of mechatronic systems, computer peripherals, and nano-manipulations. He is also a Fellow of the ASME, Chinese Society of Mechanical Engineering, the CIAE, the Robotics Society of Taiwan, and the Chinese Society of Mechanical Engineering. He received many awards, among them twice the Outstanding Research Award from Taiwan Ministry of Science and Technologies. He has served in numerous inspection committees in the government projects.

**YUNG-YAW CHEN** received the B.S. degree from the Department of Electrical Engineering, National Taiwan University, Taipei, Taiwan, in 1981, and the Ph.D. degree from the Department of EECS, University of California at Berkeley, Berkeley, in 1989. Since 1989, he has been a Faculty Member with the Department of Electrical Engineering, National Taiwan University, where he currently holds the position as a Professor. His research interests include medical robotics, automation of minimal invasive surgery, and intelligent control systems and applications.

• • •